Fuel 371 (2024) 132054

Contents lists available at ScienceDirect

Fuel

journal homepage: www.elsevier.com/locate/fuel

Full length article

Modeling homogeneous ignition processes of clustering solid particle clouds in isotropic turbulence

Pooria Farmand [a,*], Hendrik Nicolai [b], Muhammad Usman [a], Lukas Berger [a], Antonio Attili [c], Michael Gauding [a], Christian Hasse [b], Heinz Pitsch [a]

[a] RWTH Aachen University, Faculty of Mechanical Engineering, Institute for Combustion Technology, Templergraben 64, 52056 Aachen, Germany
[b] Technical University of Darmstadt, Department of Mechanical Engineering, Simulation of reactive Thermo-Fluid Systems, Otto-Berndt-Straße 2, 64287 Darmstadt, Germany
[c] University of Edinburgh, School of Engineering, Institute of Multiscale Thermofluids, The King's Buildings, Mayfield Road, Edinburgh, EH9 3FD, United Kingdom

ARTICLE INFO

Dataset link: http://dx.doi.org/10.5281/zenodo.11471198

Keywords:
Isotropic turbulence
Pulverized fuel
Ignition and combustion
DNS
Flamelet model assessment
Subgrid PDF

ABSTRACT

The objective of this study is to numerically investigate the ignition and combustion of pulverized solid fuels in turbulent conditions and to assess different modeling strategies relevant to large-eddy simulations (LES). The investigations show that due to the high Stokes number of solid particles, they do not necessarily follow the flow. At Stokes numbers around unity, particle–turbulence interactions can lead to particle clustering and change the ignition behavior. According to observations, ignition is most likely to happen outside the formed clusters, where suitable thermo-chemical conditions exist. To study this behavior, direct numerical simulations (DNS) of reactive particles in turbulent conditions employing detailed kinetics for solid and gas phases were performed. Pulverized fuel combustion was modeled using the point-particle approximation to represent the dispersed phase in an Eulerian–Lagrangian framework. Isotropic turbulence was employed to investigate the influence of particle clustering on the ignition process. After investigating the physical aspects of the ignition process, the DNS dataset was used as a benchmark for evaluating the reduced-order flamelet models usually employed in LES of pulverized fuel combustion during the ignition process. The flamelet model performance in predicting the selected quantity of interest was compared to the DNS data. An error decomposition was performed using the optimal estimator concept. Finally, the prediction accuracy of presumed PDFs is evaluated by calculating the errors in predicting the quantity of interest using different PDFs compared to the predictions using the accurate sub-filter joint distribution of the DNS data.

1. Introduction

Solid fuel combustion remains a principal technology for producing electricity, as it has reached a matured technological state and possesses reliable supply chains with the possibility of a change from conventional to bio-fuels. However, burning solid fuels, such as pulverized coal or biomass, can be a major source of pollutants and CO_2. Hence, improvements in system efficiency and carbon capture and storage (CCS) methods to reduce the environmental impact are actively researched. Experimental techniques for studying solid fuel combustion remain challenging due to the hostile environment in boilers and limited optical access [1]. Therefore, numerical simulations provide an alternative to enable insights into the underlying complex multi-physics and multi-scale processes.

For predictive modeling of solid fuel combustion, three main modeling pillars can be identified: solid fuel conversion, turbulent mixing and heat transfer, as well as turbulence–chemistry interactions [1]. For solid-fuel sub-models, most numerical studies rely on simplified models, whose parameters must be adjusted to capture fuel type changes or operating conditions accurately [1]. However, recent numerical studies have employed more detailed solid fuel models, such as the chemical percolation devolatilization (CPD) [2] or the CRECK-S [3] models [4–7]. These models enable a more detailed description of the solid particle conversion process for various fuels and a vast range of conditions by including more detailed information about the fuel, such as its molecular structure [8].

To capture the turbulent flow environment in pulverized coal combustion (PCC), traditionally Reynolds-averaged Navier–Stokes (RANS) approaches have been used. However, with the advancements of computational resources, the application of scale-resolving techniques became feasible, offering higher accuracy for predictive simulations [1,9].

* Corresponding author.
E-mail address: p.farmand@itv.rwth-aachen.de (P. Farmand).

https://doi.org/10.1016/j.fuel.2024.132054
Received 2 November 2023; Received in revised form 27 March 2024; Accepted 29 May 2024
Available online 7 June 2024

In recent years, large-eddy simulations (LES) have been successfully extended to study PCC and used in several studies [10–14]. These advancements in simulation techniques have provided valuable insights into the interactions between turbulent motion and combustion characteristics of pulverized fuels.

In the context of turbulence–chemistry interactions, state-of-the-art models are often based on a global description of gas-phase chemistry employing a limited number of reactions. Turbulence closure for these models is commonly achieved by the eddy-breakup model (EBM) or the eddy-dissipation concept (EDC) [1]. To enable a more detailed representation of the complex gas mixtures released from solid particles, recent efforts have focused on extending flamelet-based modeling approaches specifically for solid fuel combustion [15]. With different focuses, several authors have explored flamelet-based tabulation approaches with applications to various configurations ranging from single particle and particle group combustion [16,17] to pilot-scale furnaces [11–14]. Flamelet-based approaches offer the advantage of using detailed chemical mechanisms at low computational cost. They have proven effective in capturing both global characteristics, such as ignition processes [16,17], flame structures [12,13], and local species concentrations [11,14]. Particularly, in combination with LES, flamelet tabulation has shown promising results, although appropriate subgrid closures are necessary to ensure maintaining accuracy. To address the closure problem, commonly employed methods involve the use of presumed filtered density functions [1].

These presumed filter density functions can be developed and assessed by detailed reference data [18], such as direct numerical simulations (DNS), where all turbulence scales and all near- and intra-particle processes are resolved by the numerical grid. Resolving all physical processes, including the particle boundary layers, became feasible within recent years [19,20], but is still restricted to very few particles ($\mathcal{O}(10)$) and relatively low Reynolds numbers. Therefore, an alternative resolved flow simulation approach, the so-called carrier-phase DNS (CP-DNS), is commonly employed for solid fuels to enable fundamental insights into multiple interacting reactive particles. For this approach, the DNS resolves only the scales of the carrier phase, and the boundary layers around the individual particles while their impacts on the resolved scales are modeled. Using CP-DNS, Messig et al. [21] and Wen et al. [22] investigated laminar counterflow burners and performed detailed flame structure analyses for flamelet modeling; turbulent multi-phase jet burners were investigated by Luo et al. [23], Bai et al. [24], and Hara et al. [25]. These studies revealed that three distinctly different flame zones can be identified [24] and that both premixed and non-premixed combustion modes can appear [25]. Similar conclusions were drawn in the recent CP-DNS of a turbulent mixing layer resembling the condition of the inner recirculation zone of a swirled PCC boiler [26]. The latter dataset was extensively employed to evaluate different flamelet modeling approaches [27–29]. A more simplified configuration of coal particle clouds in decaying turbulence was investigated by Brosh et al. [30]. They showed a strong dependency of homogeneous ignition on particle density and clustering. Similar findings have been published for heterogeneous char conversion in forced isotropic turbulence by Krüger et al. [31]. The authors investigated turbulence-induced particle clustering and reported significant reductions in particle reactivity and char conversion rate inside particle clusters. The observed clustering effects were found to be strongly influenced by the particle Stokes number, which is the ratio of the characteristic time of a particle to the characteristic time of the flow, as indicated in the aforementioned studies. Considering that clustering occurs in larger-scale burners, it becomes crucial to investigate the performance of recently developed flamelet models and subgrid closures in the context of particle clustering.

Therefore, the objective of this work is to study the modeling of the homogeneous ignition process and volatile combustion of solid fuel particles in isotropic turbulence under conditions favoring particle clustering, which is typically observed in pulverized solid fuel burners. Particularly, the effect of particle–chemistry–turbulence interactions on the local ignition process and in clustering particle clouds is investigated. Therefore, modeling strategies for both the reduction of the gas-phase reactions by an FPV approach and the required closure for the filtered variables in the context of LES are studied in homogeneous isotropic turbulence-induced particle clusters. The optimal estimator concept is employed to determine modeling errors and provide an effective modeling strategy for turbulent solid-fuel combustion.

The remainder of the paper is structured as follows. First, in Section 2, the employed numerical framework and the models to be assessed are briefly introduced. This is followed by a short description of the numerical setup and the boundary conditions for the DNS in Section 3. In Section 4, first, the physical effects of the employed configuration are presented, then a combined LES-FPV approach is assessed in an *a priori* analysis.

2. Modeling framework and methods

2.1. Multi-phase modeling

In this study, the ignition and combustion process of pulverized coal particle clouds is represented by an Eulerian–Lagrangian approach. The conservation of mass, momentum, species, and energy between the Lagrangian and Eulerian frameworks is ensured by a two-way coupling. Utilizing the two-way coupling also ensures the particle–fluid–chemistry interactions by distributing the particles' source terms in the Eulerian phase and calculating the gas-phase quantities at the particles' location. The detailed description of the models and the equations for the Eulerian and Lagrangian formulations can be found in Farmand et al. [5] and Farazi et al. [32]. The accuracy of the applied models and methodologies have been validated against experimentally measured data for ignition times in different laminar configurations in earlier works [5,32–34]. One particular focus of these studies was on properly capturing particle movement and ignition of point particles on DNS grids through a Gaussian kernel source term distribution. Chemical reactions in the gas phase are described employing finite-rate chemistry adopting a mechanism suitable for coal and biomass combustion with 68 species and 906 reactions, which has been validated for different fuels in both air and oxy-fuel atmospheres [35], and has been used in previous studies [4,5,36,37].

Particle dynamics are modeled in a Lagrangian framework using the point-particle assumption solving equations for trajectory, velocity, mass, and temperature as described in previous works [5,32,38]. In order to have a detailed description of the solid particle conversion, the chemical percolation devolatilization (CPD) model, which is one of the most detailed models for solid kinetics, is used to describe the volatile release from the solid particles based on the molecular structure of the fuel and considers the solid fuel as a complex network of the large aromatic hydrocarbon monomers and the bridges, in which bonds are broken by the external energy at each temperature level. This model, as described in detail in [2,8,39], takes into account the dynamic behavior of the devolatilization process by determining total released mass as well as its composition in light gases and tar. In the present study, light gases consist of CH_4, CO_2, CO, H_2O, and other gases, which are assumed to be C_2H_2 similar to the assumption by Jimenez and Gonzalo-Tirado [40]. The released tars are assumed to solely consist of C_2H_2. To reduce the level of complexity in the model assessment procedure, similar to [5], a fixed volatile composition assumption (FVC) is employed for the particle devolatilization in the CPD model. The FVC is calculated based on the time-averaged values of each volatile species' mass compared to the total released mass from the particle [4]. The resulting set of fixed volatile mass fractions is $Y_{CH_4} = 0.057$, $Y_{CO_2} = 0.072$, $Y_{CO} = 0.087$, $Y_{H_2O} = 0.268$, and $Y_{C_2H_2} = 0.516$. Assuming a fixed volatile composition neglects the relationship between the change in particle heating rate and the volatile release, which is commonly made

for flamelet modeling in the LES of solid pulverized fuel flames [4] and was found to only marginally affect ignition [5].

To solve the governing equations in isotropic turbulence, the in-house structured finite difference solver CIAO is used. In CIAO, the Eulerian equations are solved using a semi-implicit scheme with second-order accuracy in space and time. The scalar transport is solved using the fifth-order WENO scheme for the convective terms and a second-order central difference scheme for the diffusive terms. The chemistry is solved using the finite rate chemistry method using the CVODE solver [5,32]. The particles are advanced in time utilizing a two-stage Runge–Kutta solver with second-order accuracy to update the dispersed phase state, position, and source terms for the Eulerian equations. The reader is referred to previous works for specific details on the numerical implementation [5,32].

2.2. Flamelet library for a priori analysis

To model the turbulent reacting gas-phase in solid fuel combustion, flamelet-based tabulation methods are gaining attraction due to the possibility of including detailed kinetics in large-scale simulations. In this work, flamelet tables, which are used for the *a priori* model assessment in post-processing, are built from counterflow-diffusion flamelets, which matches the non-premixed nature of combustion in the current study configuration. These are solved in physical coordinates using Cantera [41], assuming unity Lewis numbers for all species, which is a common assumption in PCC (e.g., [4,14]). The same gas-phase kinetic model as for the DNS is used to calculate the flamelets [35]. During the flamelet calculation, the strain rate is varied by changing the inflow boundary conditions. For the tabulation process, the varying strain rates are mapped onto a progress variable (C) [42], which represents the combustion progress.

To take into consideration heat losses in the gas-phase caused by particles and radiative heat transfer, the enthalpy h (sensible plus chemical) is introduced as an additional table dimension, and flamelets with different enthalpy levels are computed. For higher enthalpy values, the temperatures of the oxidizer and fuel are increased (from 300 K up to 1500 K). To obtain lower enthalpies, the source term in the temperature equation in Cantera is rescaled, as proposed by several authors [4,14,43]. Below a certain enthalpy level, no flamelet solution can be obtained. Here, a linear extrapolation to 300 K is used to complete the composition space [16,44].

In the flamelet tabulation, normalized values for h and C based on the lower and upper limits of the flamelet table, which represents the lowest and highest possible temperature for the composition space, are employed [45]:

$$C_\mathrm{n} = \frac{C - C_\mathrm{min}(h,Z)}{C_\mathrm{max}(h,Z) - C_\mathrm{min}(h,Z)}, \tag{1}$$

$$h_\mathrm{n} = \frac{h - h_\mathrm{min}(Z)}{h_\mathrm{max}(Z) - h_\mathrm{min}(Z)}. \tag{2}$$

This will also improve the statistical independence between table input parameters [42,46] and enable the possibility of evaluating different presumed PDF shapes for all input parameters when coupled to LES.

When the tabulated chemistry is coupled to LES, modeling of the subgrid filtered/probability density functions (FDF/PDF) is required since only Favre-filtered scalars are available for the table access [42]. Closure can be obtained through the joint-scalar-PDF in composition space. This involves integrating the joint-scalar-PDF over the composition space to obtain the filtered quantity of interest as

$$\bar{\Psi} = \int \Psi\left(Z, C_\mathrm{n}, h_\mathrm{n}, \ldots\right) \tilde{P}\left(Z, C_\mathrm{n}, h_\mathrm{n}, \ldots\right) dZ dC_\mathrm{n} dh_\mathrm{n} \ldots, \tag{3}$$

where the density-weighted PDF $\tilde{P}$ follows from the Favre-averaging procedure. Since the joint-scalar-PDF is computationally expensive to calculate during runtime, presumed PDF closures are commonly employed. The PDF has to be parametrized by the moments of the distribution, and it is often assumed that the PDF can be represented by its first two moments. Since prescribing a feasible presumed PDF for the joint PDF of multiple scalars is very challenging, the simplified assumption of statistical independence between the scalar dimensions of the joint PDF is often used [14,18]. As a result, the representation of the joint PDF of multiple scalars in composition space can be facilitated to the product of the individual marginal scalar PDFs as:

$$\bar{\Psi} = \int \Psi\left(Z, C_\mathrm{n}, h_\mathrm{n}\right) \tilde{P}\left(Z, \tilde{Z}, \widetilde{Z''^2}\right) \tilde{P}\left(C_\mathrm{n}, \tilde{C}_\mathrm{n}, \widetilde{C''^2_\mathrm{n}}\right) \tilde{P}\left(h_\mathrm{n}, \tilde{h}_\mathrm{n}, \widetilde{h''^2_\mathrm{n}}\right) dZ dC_\mathrm{n} dh_\mathrm{n} \tag{4}$$

Mostly, in tabulated flamelet models used in pulverized fuel combustion, all scalars besides the mixture fraction are modeled by a δ function, and the sub-grid PDF of the mixture fraction is approximated by top-hat [6,47] or β [4,14] distribution functions.

2.3. Error decomposition analysis

The modeling of unclosed terms in partial differential equations typically involves two steps: First, a set of known quantities needs to be specified as input parameters for a model, and second, a specific functional form needs to be defined to model the unclosed terms by the input parameters [48–50]. Each of these steps introduces errors that need to be carefully investigated in the model assessment process. The error corresponding to the first step is known as the irreducible error, and the error corresponding to the second step is referred to as the functional error. Typically, the total modeling error, which involves both irreducible and functional errors, is calculated by the overall difference between quantities of interest calculated by the model and the DNS. The quadratic total modeling error over all N data points is defined as

$$\epsilon^2_\mathrm{tot}(\phi) = \frac{1}{N}\sum_{i=1}^{N}\left(\phi_{i,\mathrm{DNS}} - \phi_{i,\mathrm{Model}}\right)^2, \tag{5}$$

where $\epsilon_\mathrm{tot}(\phi)$ is the average value of the total modeling error for a quantity of interest ϕ over all N data points. The general idea of the optimal estimator concept is to determine for a given parameter set Π, the mean of a quantity of interest ϕ conditioned on the set of parameters $\langle\phi \mid \Pi\rangle$ and obtain a measure for the scatter of the quantity of interest with respect to Π. This is the minimum error possible after choosing the parameters set and is called irreducible error. In this study, an artificial neural network (ANN) with a single hidden layer is used to calculate the optimal estimator and the irreducible error, which is computationally efficient, even when using a large number of input parameters [48].

Using the optimal estimator and the irreducible error concepts, the total modeling error can be decomposed into irreducible and functional errors [48], in which the functional error corresponds to the performance of the model for a given input parameter set

$$\epsilon^2_\mathrm{tot}(\Pi) = \epsilon^2_\mathrm{irr}(\Pi) + \epsilon^2_\mathrm{funct}(\Pi), \tag{6}$$

where Π is a set of known parameters used as input of the model. Formally, the irreducible error is given as

$$\epsilon^2_\mathrm{irr} = \left\langle\left(Q_\mathrm{int} - \langle Q_\mathrm{int} \mid \Pi\rangle\right)^2\right\rangle \tag{7}$$

In the following, irreducible error ϵ_irr and the error caused by the functional form of the model ϵ_funct, as defined by Eq. (6), will be discussed separately for identifying the potential for model improvements.

2.4. Quantifying preferential concentration/clustering

When the particles are exposed to turbulence, their trajectory depends on the turbulent intensity and particle inertia. This can lead to a local increase in the particle number density at specific locations in the field, which is known as preferential concentration or clustering [51,52]. To identify the formed clusters, the three-dimensional

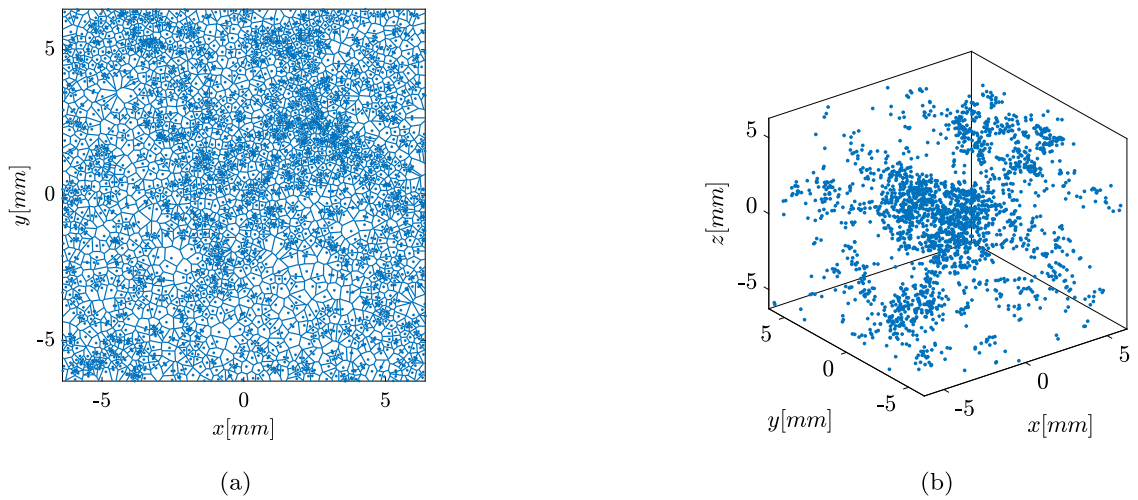

Fig. 1. (a) Voronoi tessellation diagram for the 2D slice of the box (b) Cluster member particles filtered by the Voronoi algorithm at the initial time of the clustering.

Voronoi tessellation method is employed [53]. In this method, the 3D particle field is discretized by Voronoi diagrams created by the half-plane intersection algorithm between each two particles in the field. This results in a specific volume around each particle, called Voronoi cells, as described in [53]. The size of each Voronoi cell is inversely related to the local concentration of the particles in a certain location in the field [54]. After discretizing the domain by the Voronoi cells, the clustering limit V_C can be obtained by comparing the normalized Voronoi volume distribution in the clustered field $P(V/\overline{V})$ with a randomly distributed particle field $P(V_R/\overline{V})$, in which $\overline{V}$ in the mean Voronoi cell volume in the selected field, which is calculated based on the Voronoi volume around each particle as described in [53]. V_C can be calculated when $P(V/\overline{V}) = P(V_R/\overline{V})$. A more detailed description of the method can be found in Obligado et al. [52] and Monchaux et al. [53]. After performing the Voronoi algorithm as shown in Fig. 1a, a particle can be a member of a cluster when the respective Voronoi volume around the particle is smaller than the calculated clustering limit (V_C). As a result, the cluster members can be identified as shown in Fig. 1b.

3. Numerical setup and boundary conditions

In order to reduce the complexity caused by mean shear forces, it is preferred to keep the turbulence fluctuations statistically uniform so that all particles are subjected to the same turbulence statistics. Therefore, the homogeneous isotropic turbulent (HIT) configuration within a box with periodic boundary conditions in all directions is chosen. Due to the absence of mean gradients, HIT has no turbulence production, and, as a result, turbulence decays in time. To investigate the effect of turbulence interactions on the ignition and the combustion process, a pre-computed fully developed HIT field with a linear forcing in physical space [55] is used as initial conditions to keep turbulence in a statistically steady state. Simulations were performed within a region with the physical size of 12.8 mm × 12.8 mm × 12.8 mm with periodic boundary conditions in all directions. The domain size is discretized with a three-dimensional cartesian mesh with a resolution of $\Delta x = 50$ μm. Since the particle clustering effect on ignition is one of the main aspects of this study, turbulence characteristics and dispersed phase size have been chosen such that particle clustering can be observed. These conditions are representative of smaller-scale turbulent fluctuations under practically relevant conditions [7,26].

Particle clustering typically occurs when the characteristic time of the particles is on the same order as the flow time scale and is defined by the Stokes number. For Stokes numbers around unity, particles tend to form clusters, resulting in regions almost void of particles [56]. The Stokes number defined with the Kolmogorov time scale is given as

$$St = \frac{\rho_{prt} {d_{prt}}^2}{18 \rho_g \eta^2}. \tag{8}$$

A forced isotropic turbulent field with $Re_\lambda \simeq 30$ and the Kolmogorov length scale $\eta \simeq 100$ μm has been chosen. The dispersed phase consists of 10,000 particles of Colombian coal with $d_{prt} = 20$ μm and $T_{prt,0} = 300$ K and with apparent density of 700 kg/m^3. The coal properties can be found in [5]. Non-reactive particles are first randomly distributed in the box filled with air with 20% oxygen and an initial gas temperature of $T_{g,0} = 1500$ K, which is relevant to practical PCC applications. Based on Eq. (8), these conditions lead to an initial Stokes number of $St \simeq 5$, for which a clustering behavior in particle clouds motion is expected [57]. Finally, the reactive simulation starts after particle clusters have fully formed in a non-reactive HIT field to investigate the effect of particle clustering on the homogeneous ignition process. The employed forced isotropic turbulence ensures maintaining the same turbulence statistics during non-reactive and reactive simulations as summarized in Appendix.

To quantify the ignition process, an ignition criterion needs to be defined. Typically, in joint numerical–experimental studies, a certain OH radical threshold is chosen as an ignition identifier based on OH-LIF measurements [5,34]. In the current study, due to non-existing experimental measurements for the current complex configuration, the same definition, used in previous studies [5,16] to quantify the ignition process was used to have a realistic benchmark for the analysis. This definition has been validated against the experimentally measured ignition delay time in previous works. As a result, the ignition onset is defined as the time when 10% of the maximum OH mass fraction during the entire combustion process is reached.

4. Results and discussion

In the following sections, first, the physical aspects of the ignition of clustering particles in isotropic turbulence and the ignitability condition are investigated. Then, the available models and their applicability for the ignition prediction in the clustering particle clouds are assessed.

4.1. Ignition process of clustering particles in isotropic turbulence

Fig. 2 shows the evolution of the ignited regions in the computational domain over time. As shown in Fig. 2a, various ignition kernels are formed at various locations within the field where favorable thermo-chemical conditions for ignition exist. This process continues with the ignition of the adjacent regions due to the growth and merging

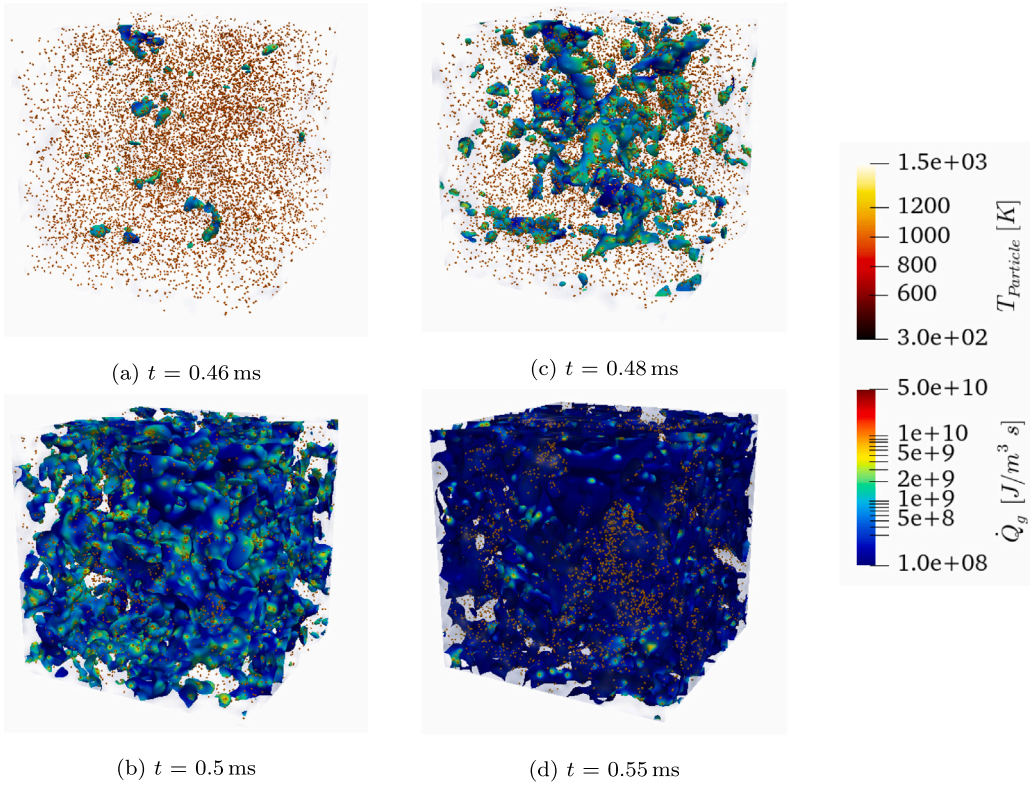

Fig. 2. Snapshots of the ignition process illustrated by the iso-surfaces of the 10% of the maximum OH mass fraction during the entire combustion process ($Y_{OH,max}$) colored by heat release. Particles are shown with points colored by particle temperature. (For interpretation of the references to color in this figure legend, the reader is referred to the web version of this article.)

of individual ignited regions until the whole domain is ignited and a continuous flame is established. The transition from the auto-ignition regime to the flame front propagation mode, which in this study is referred to as interaction ignition [58], can be quantified by investigating the time evolution of the ignited regions in the field as shown in Fig. 2.

Fig. 2a also indicates preferential particle concentration, also known as particle clustering. To further investigate this observation, Voronoi regions are introduced to study the effect of particle clustering in the ignition and combustion process. The ignition is investigated in each Voronoi region, following the definition given in Section 2.4. When particle clusters form in the turbulent field, the local particle number density increases at specific volumes, and the local gas temperature decreases due to the energy sink required for clustered particles heat-up at those locations. Therefore, the thermo-chemical conditions are more suitable for ignition in the location outside of the clusters, and as a result, the first ignition kernels are observed mostly in those regions. This behavior is quantified in Fig. 3 with respect to the normalized Voronoi volumes. Fig. 3a shows the number of ignited cells $N_{\text{ign,cell}}$ normalized by the total number of cells in the numerical domain $N_{\text{cell,tot}} = 256^3$, where a higher number of ignited points can be observed at volumes larger than V_C. Also, Fig. 3b shows an overall higher gas-phase temperature at volumes larger than V_C. Recall that larger Voronoi volumes indicate lower local particle number density, which is typically found outside of particle clusters.

After investigating the position of the individually ignited regions, the complete transient ignition process shown in Fig. 2 is quantified by calculating the number of the ignited regions and their corresponding volumes during the ignition process. Fig. 4a shows an increase in the number of auto-ignited regions from $\tau_{\text{auto.ign}} \simeq 0.46$ ms until $\tau_{\text{int.ign}} \simeq 0.5$ ms. At this point, no new individual ignition kernels are formed. Subsequently, ignition kernels start to merge, leading to a decrease in the number of separate ignited regions. Simultaneously, the total volume of the ignited regions starts to expand rapidly due to flame propagation. This mode of ignition was recently introduced as interaction ignition [58].

To compare the correlation between the ignition region and turbulent scales, the Kolmogorov length (η) is utilized as a reference length. Fig. 4b shows the PDF of the ignited region length scale l_{ign} normalized by the Kolmogorov length for different instances of the ignition process. The ignited region length scale is defined by assuming a spherical shape for the ignited region $l_{\text{ign}} = (6/\pi)V_{\text{ign}}^{1/3}$. Ignition kernels with different sizes are indicated by the broad PDF shape at $t = 0.46$ ms and $t = 0.5$ ms. After the ignition regions merge ($t > 0.5$ ms), the PDFs become narrower, suggesting that the regions converge towards a certain size. According to the corresponding distributions for $t > 0.5$ ms, the PDF shows a weak bimodal behavior. The prominent peak corresponds to the individual kernels and the large value of the PDF for large ignition lengths corresponds to the merged kernels. Later in the ignition process, the peak corresponding to the individual kernels shifts to smaller ratios, and the PDF value in the far right grows, indicating an increase in the number of merged kernels. An interesting observation is that the size of the ignited regions consistently remains around one order of magnitude larger than the Kolmogorov length scale. This is promoted due to the fact that ignition happens primarily outside of the particle clusters, where a more uniform volatile-oxidizer mixture with suitable thermo-chemical conditions for ignition exists and can be ignited on larger length scales.

In order to study the suitable thermo-chemical conditions for ignition, the mixture fraction and scalar dissipation rate concepts are utilized. Mixture fraction indicates the amount of local volatile/oxidizer mixing and the scalar dissipation rate represents the local rate of diffusive mixing at the molecular level, and therefore, it is a key element for the modeling of turbulence–chemistry interaction. Fig. 5 provides insights into the ignition conditions, utilizing the scalar dissipation rate

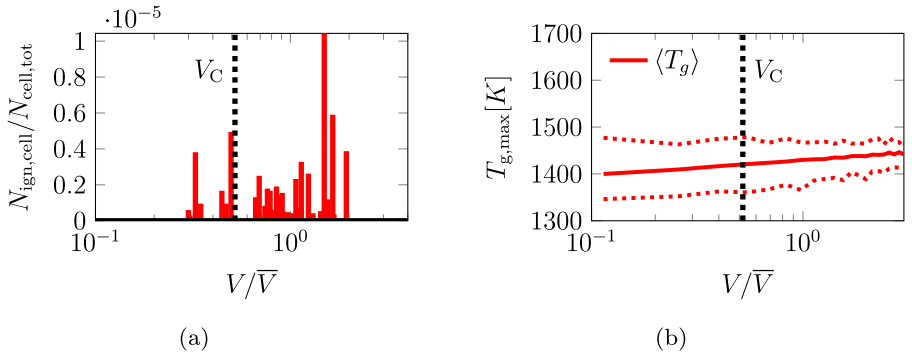

Fig. 3. (a) Normalized number of the ignited cells and (b) gas temperature in normalized Voronoi volumes at $\tau_{\mathrm{auto.ign}} \simeq 0.46$ ms. Red dotted lines show the minimum and maximum gas temperature in normalized Voronoi volumes. Volumes larger than V_C represent regions outside of clusters. (For interpretation of the references to color in this figure legend, the reader is referred to the web version of this article.)

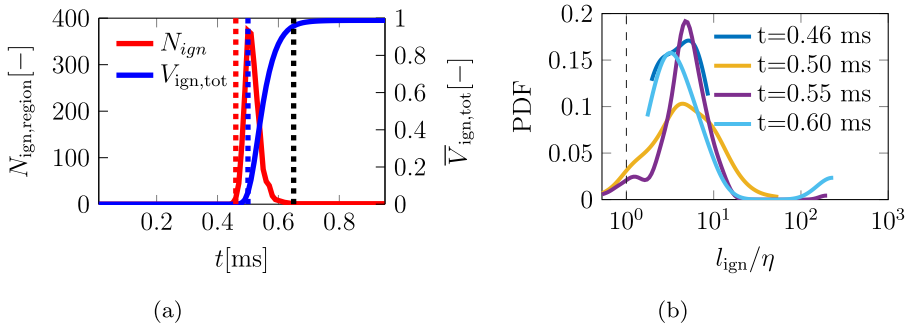

Fig. 4. (a) Evolution of the number of separated ignited regions (N_{ign}) and the total normalized volume $\sum V_{\mathrm{ign}}$ of the ignited regions. The vertical red, blue, and black dotted lines show the auto-ignition time, interaction ignition time, and end of the ignition process, respectively. (b) Distribution of the ignited region length scale compared to the Kolmogorov scale η. The vertical dashed line corresponds to the Kolmogorov length scale. (For interpretation of the references to color in this figure legend, the reader is referred to the web version of this article.)

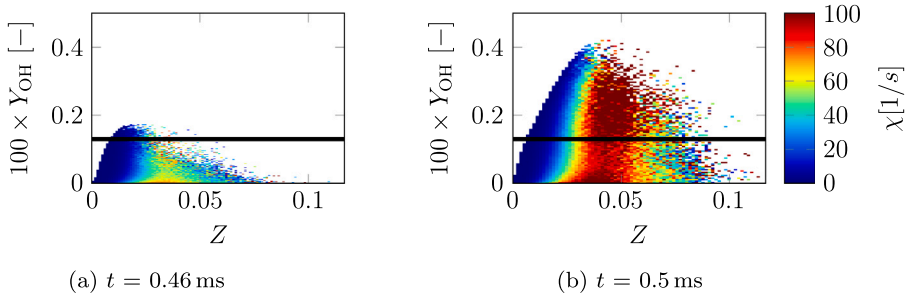

Fig. 5. OH mass fraction and mixture fraction colored by the scalar dissipation at $t = 0.46$ ms and $t = 0.5$ ms. The horizontal black line shows the ignition threshold for OH mass fraction based on the ignition definition.

and mixture fraction calculated based on Bilger's definition, revealing that the ignition process primarily takes place in lean mixtures ($Z \sim 0.02$), specifically away from the particles. Considering the fixed volatile composition assumption [5] for the released volatiles and their global reaction with the oxidizer, the stoichiometric mixture fraction is $Z_{st} = 0.117$. This observation aligns with the findings from the Voronoi analysis. Larger Voronoi volumes indicate locations outside of a cluster that leads to lower released volatiles and, as a result, a lower amount of fuel in ignited regions. Additionally, Fig. 5a shows that at $\tau_{\mathrm{auto.ign}} \simeq 0.46$ ms, some locations in the domain, characterized by the same mixture fractions, do not undergo ignition. Notably, for a given mixture fraction, regions with smaller scalar dissipation rate ignite first.

As shown in Fig. 5b, at later times during ignition ($\tau_{\mathrm{int.ign}} \simeq 0.5$ ms), locations with higher scalar dissipation rates also ignite at higher mixture fractions, which are closer to the clusters, where volatiles are released. Also, high scalar dissipation rates near the clusters (higher mixture fractions) promote mixing, leading to a premixed mixture of volatiles and the oxidizer, which facilitates premixed flame propagation from the ignited regions toward the clusters.

The particle clouds ignition process is inherently transient, and the presence of particle clustering further affects the reactivity [31]. Therefore, it is crucial to carefully evaluate the assumptions made in reduced-order models for ignition and combustion to predict important flame characteristics in this particular configuration.

4.2. A priori model assessment of clustering particle clouds in the prediction of the ignition process

In this section, a systematic assessment based on error decomposition is used to evaluate the overall performance of the model from different perspectives. First, the performance of the tabulated chemistry in a flamelet/progress variable (FPV) model compared to DNS is studied to quantify the suitability of the tabulated thermo-chemical state. Second, the presumed PDF used to pre-integrate the table is compared

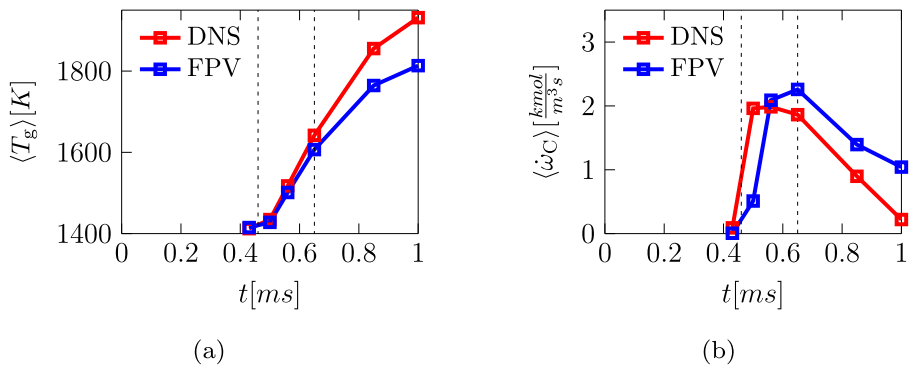

Fig. 6. Overall comparison between the DNS data and the FPV model in predicting the volume-averaged (a) gas temperature, and (b) progress variable source term at different times. Vertical dotted lines indicate the start and end of the ignition process based on Fig. 4a.

with the filtered DNS dataset to find the optimal presumed PDF shapes for each input parameter of the table.

The reference progress variable is defined as [4]

$$C_{\text{ref}} = \frac{Y_{CO_2}}{\mathcal{M}_{CO_2}} + \frac{Y_{CO}}{\mathcal{M}_{CO}} - \frac{Y_{O_2}}{\mathcal{M}_{O_2}}, \tag{9}$$

where $\mathcal{M}_i$ is the molar mass of species i.

The total modeling errors are systematically decomposed into the functional and irreducible errors employing the optimal estimator method described in Section 2.3.

4.2.1. Assessment of the thermo-chemical states in tabulated chemistry

In order to have a general overview of the FPV model performance, the volume-averaged $\langle T_g \rangle$ and $\langle \dot{\omega}_C \rangle$ in the entire domain at different times during ignition and combustion are calculated, according to the model described in Section 2.2 and compared with the DNS data. To calculate a volume-averaged quantity $\langle \phi \rangle$ in the DNS and the FPV model, the following equation is used

$$\langle \phi(t) \rangle = \frac{1}{N} \sum_{i=1}^{N} \left(\phi_i(t) \right), \tag{10}$$

where N is the total number of cells in the entire volume. As illustrated in Fig. 6, the comparison between the model and reference data shows good overall agreement in gas temperature, although increased deviations are apparent for later times. Comparing the progress variable source term shows a shift in the prediction of the FPV model compared to the DNS, which indicates later ignition delay time prediction by the model. However, nearly the same peak average value of the progress variable source term is observed in the FPV model. In order to investigate the differences during the ignition process, the progress variable source term ($\dot{\omega}_C$) is chosen as the quantity of interest for modeling particle cloud ignition and combustion processes in isotropic turbulence.

To understand the origin of the deviations in the FPV model from the DNS results, the performance of the model inside and outside of the particle clusters is studied in more detail. To this end, two different time instances, $t = 0.5$ ms with the maximum number of ignited regions during the ignition process and $t = 0.65$ ms, which is at the end of the ignition process, as shown in Fig. 4a, are chosen. First, the model parameters chosen to parameterize the flamelet table are assessed by the optimal estimator method. This enables calculating the irreducible errors for different sets of input parameters for predicting the quantity of interest. To obtain a meaningful value for the errors with respect to particle cluster locations, they are normalized by the maximum value of the conditionally averaged quantity of interest in the normalized Voronoi volumes ($V/\overline{V}$).

$$\overline{\epsilon} = \frac{\sqrt{\epsilon^2}}{\max(\langle\, Q_{int} \mid V/\overline{V} \rangle)}. \tag{11}$$

Different combinations of mixture fraction, progress variable, and enthalpy, as well as the OH mass fraction, as it is one of the most important ignition identifier species, are used to find the best possible set of parameters to characterize the composition space.

After comparing the different combinations, Fig. 7 demonstrates that the inclusion of the progress variable and enthalpy alongside the mixture fraction strongly decreases the overall irreducible error, especially inside the clusters at early times, where the errors are highest. It is interesting also to note that consideration of enthalpy is not needed if only the chemical source term is of interest. Including Y_{OH} as an input parameter leads to a slight improvement in the overall irreducible error. However, the error corresponding to Z, C_n, Y_{OH} is still comparable with the error corresponding to Z, C_n and Z, C_n, h_n. Also, creating a table with OH radical, which can perform well in the *a posteriori* LES, is very challenging, since OH radical is not readily available in LES. As a result, in this study, this radical is not considered as an additional input parameter.

Next, the functional errors are assessed at $t = 0.5$ ms and $t = 0.65$ ms. Using the parameters Z, h_n, and C_n, as discussed earlier, a flamelet table is generated. The quantity of interest from the table are compared with the corresponding values from the DNS datasets to calculate the functional errors based on Eqs. (5) and (6).

Fig. 8 compares the progress variable source term between the flamelet table and the DNS. The tabulated flamelet model exhibits certain limitations in accurately predicting $\dot{\omega}_C$, particularly within the particle clusters.

Comparing the model performance at two different time instances shows that for $\dot{\omega}_C$ the modeling error is higher at ignition. The increased functional error observed during the ignition process primarily occurs within the particle clusters, specifically in close proximity to the particles themselves. This can be attributed to the limitations of the typically used flamelet tables in capturing the particle–chemistry interactions due to the fact that the particle effects in the flamelet table are not considered. This limitation is especially prominent in the vicinity of particle clusters, which corresponds to a smaller mixing time scale compared to the chemical time scale. In these regions, where the volatiles mix with the oxidizer prior to ignition, the flame behavior resembles that of a premixed flame, which cannot be accurately captured by the non-premixed flamelet approach employed in this study.

After assessing the reference FPV model's input parameters and its performance in predicting the quantity of interest, the effects of changing the input parameters, such as excluding enthalpy and altering the progress variable definition in the model performance, are examined next.

4.2.2. Effect of heat losses in flamelet tabulation

In order to investigate the effect of heat losses in the table, a table with two input parameters (Z and C_n) is generated. Its performance is compared with the reference FPV model (Z, C_n, and h_n). From Fig. 9,

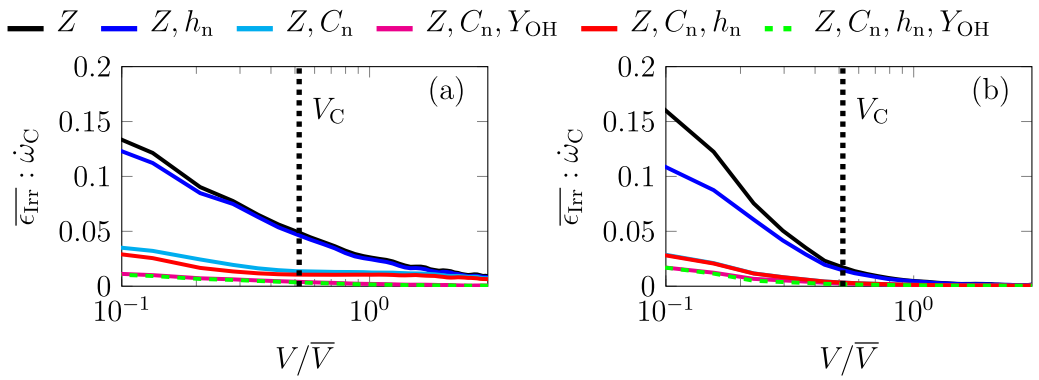

Fig. 7. Irreducible errors of different input parameters in predicting progress variable source term at (a) t = 0.5 ms and (b) t = 0.65 ms. Volumes larger than V_C represent regions outside of clusters.

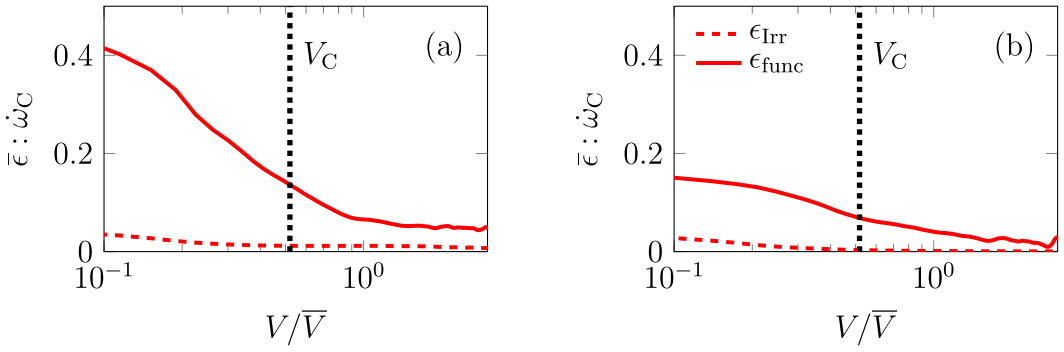

Fig. 8. Errors involved in the reference FPV model in comparison with the DNS results in the prediction of progress variable source term at (a) t = 0.5 ms and (b) t = 0.65 ms. Volumes larger than V_C represent regions outside of clusters.

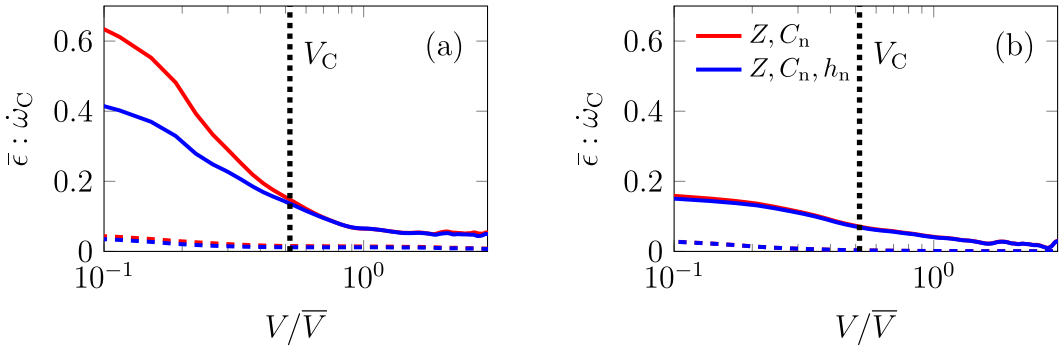

Fig. 9. Effect of enthalpy in the errors of progress variable source term at (a) t = 0.5 ms and (b) t = 0.65 ms. Solid color lines show the functional errors and dashed color lines are the corresponding irreducible errors. Volumes larger than V_C represent regions outside of clusters. (For interpretation of the references to color in this figure legend, the reader is referred to the web version of this article.)

it is evident that including enthalpy in the table primarily affects the predictions.

The results demonstrate that incorporating enthalpy as an input parameter improves the accuracy inside the clusters, particularly during ignition. This suggests that the ignition phase is more sensitive to changes in enthalpy compared to later stages of combustion, especially inside the clusters. During the ignition phase, due to the particle heat-up process and the higher temperature gradients between particles and the gas phase, the heat loss effect is more dominant than at later times [16].

4.2.3. Effect of progress variable definition

In this section, the effect of altering the progress variables definition on model performance is investigated. To this end, three different progress variables, as defined in Table 1, are compared with the reference definition (C_{ref}) in Eq. (9). These definitions are employed to compare the typically used definitions in flamelet tabulated chemistry models [4,7] for pulverized solid fuel combustion and to investigate the effect of removing certain species from the progress variable definition.

Table 1
Different progress variable definitions.

C	Definition
C_1	$Y_{CO_2} + Y_{CO}$
C_2	$Y_{CO_2} - Y_{O_2}$
C_3	$Y_{CO_2}/\mathcal{M}_{CO_2} + Y_{H_2O}/\mathcal{M}_{H_2O} - Y_{O_2}/\mathcal{M}_{O_2}$

Fig. 10 shows the effect of progress variable definition on the overall model performance. It can be observed that excluding CO or O_2 from

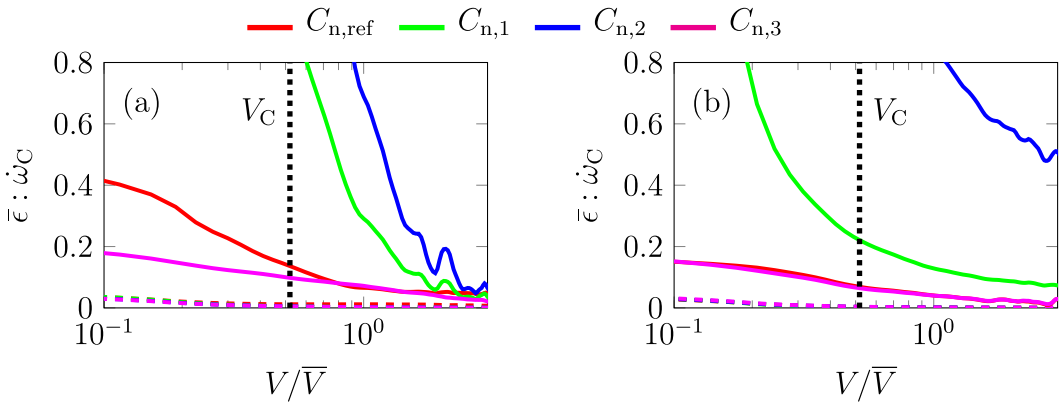

Fig. 10. Effect of progress variable definition in the errors of progress variable source term at (a) t = 0.5 ms and (b) t = 0.65 ms. Solid color lines show the functional errors and dashed color lines are the corresponding irreducible errors. Volumes larger than V_C represent regions outside of clusters. (For interpretation of the references to color in this figure legend, the reader is referred to the web version of this article.)

the model significantly amplifies the functional errors of predicting the progress variable source term ($\dot{\omega}_C$), indicating that C_1 and C_2 are not suitable choices for representing the progress variable. On the other hand, replacing CO with H_2O (C_3) resulted in an improvement in predicting the quantity of interest, particularly within the clusters.

4.2.4. Assessment of the presumed PDF shapes in comparison with subgrid scalar PDF

In the context of LES, only filtered scalars are transported, which cannot be used directly for table access. The unresolved subgrid distribution of the transported scalars is often modeled by a presumed-β PDF for the mixture fraction Z, whereas the distributions of the remaining scalars are modeled by a δ function [1,14]. These assumptions will be examined in the following by employing different presumed PDF shapes for the table input parameters. By comparing the results to the DNS data, the suitability of considering subgrid-scale fluctuations can be analyzed.

In order to evaluate the model performance when coupled to LES, the DNS dataset is filtered using a box filter of width $\Delta_f = 8\Delta x$, ensuring an averaged resolved energy of about 90% with respect to the DNS field, which is a typical value for a well-resolved LES [59]. After filtering, the distribution of the input parameters (Z, h_n, C_n) from the DNS is examined to determine suitable PDF shapes that accurately represent the behavior of each input parameter. In Fig. 11, various PDF shapes (δ, β, and Top-hat (TH) distributions), which are widely used in the pulverized solid fuel modeling [4,6,22,47], based on the Favre-averaged mean and variance of the filtered dataset are compared with the distribution of the input parameters obtained from the DNS dataset at two different time instances within a specific filter cell of the DNS field.

It should be noted that in the context of point-particle DNS, distributing the particles' source term over a specific kernel shape can impact the evolution of the mixture fraction PDF. Distributing the source term across a Gaussian kernel, a technique applied to better account for finite size effects of particles [32,38,60] results in a broader source term distribution, diminishing peak values on the fuel side. Consequently, both the mean and variance of the mixture fraction decrease, affecting the PDF shape. However, it is expected that the overall shape of the PDF remains similar, and only the width of the distribution would be affected by the distribution of the source term compared to fully resolved simulations, which incorporate particle boundary layer effects. Incorporating boundary layer effects into the present study, as evidenced by Wang et al. [61], would complicate the model assessment procedure and require further investigation using fully resolved simulations. However, considering the finite-size particle effects ensures a more realistic benchmark for the subgrid scalar PDF assessment.

Comparing different presumed PDF shapes based on Fig. 11 shows that all presumed approaches have difficulties in approximating the DNS distribution. Top-hat distributions are symmetrical with respect to the mean and, as a result, cannot capture the non-symmetrical DNS, which is originated from the particle clustering effects. Mixture fraction distribution shows higher probabilities in smaller mixture fractions, which is due to more data points outside of clusters. It can also be observed that for the mixture fraction, as suggested in the original formulation for single-phase combustion [42], the β distribution yields a more accurate distribution than other PDF shapes compared to the DNS for clustering particle cloud ignition.

To complement the qualitative investigation of the presumed PDF shapes shown in Fig. 11, the errors involved in the model when using presumed PDF assumption during clustering particle cloud ignition and combustion is evaluated. Since the selected PDF shapes can be represented by the first two moments, meaning mean and variance, incorporating different PDF shapes for mixture fraction, progress variable, and enthalpy would require their mean and variance as inputs of the model. It should be noted that utilizing higher-order moments can lead to a more accurate representation of the DNS distribution. However, this can lead to a further increase in the table dimensions. In order to determine the optimal input sets, including the variances, the concept of optimal estimator is employed to calculate the irreducible error associated with each set.

Fig. 12 shows the irreducible error for predicting the filtered progress variable source term using different sets of input parameters, including variances. It can be observed that at ignition, adding the variances to the reference Favre-averaged input set ($\tilde{Z}$, $\tilde{C}_n$, $\tilde{h}_n$) does not improve the results very much. This shows that the model is not sensitive to variances of input parameters at ignition. The mixture fraction distribution in Fig. 11 shows a smaller variance during ignition compared to the end of ignition due to a lower total volatile release. Also, considering variances of progress variables and enthalpy is not sufficient for the correct prediction of the quantity of interest in the filter cells at ignition.

It should be mentioned that at t = 0.65 ms, adding variances to the reference input set improves the irreducible error. This improvement in the prediction is due to the larger variances (especially $\widetilde{Z''^2}$) and non-linearity of the progress variable source term with respect to input parameters in the filter cells.

After analyzing different input parameter sets and studying the effect of PDF shape on irreducible error, it is necessary to investigate the impact of including variances in the functional errors for predicting the filtered quantity of interest. The non-symmetrical characteristic of the DNS distribution due to particle clustering can be better represented by a β-PDF. Therefore, this study focuses on investigating the performance

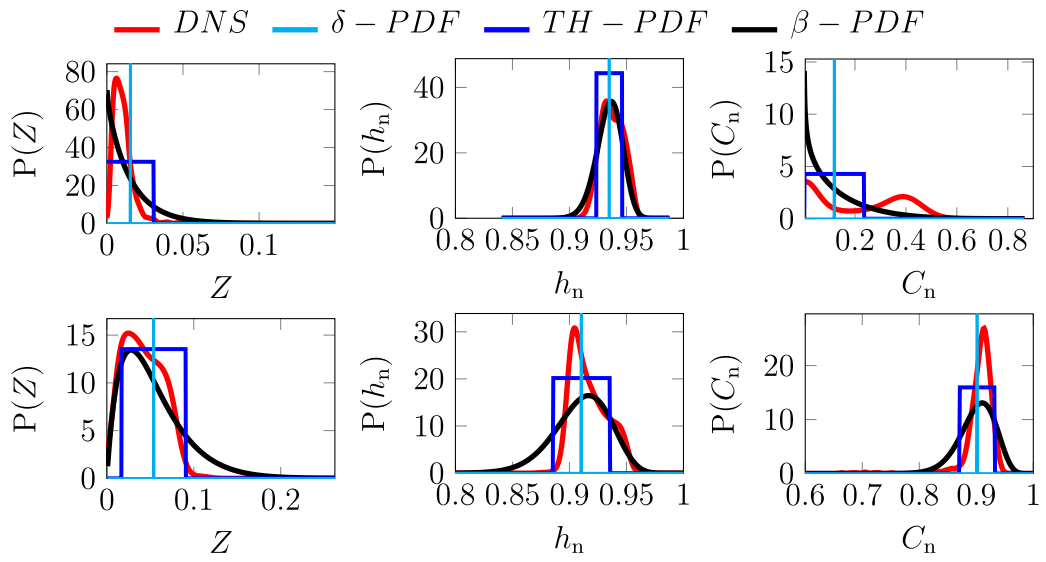

Fig. 11. Comparing different presumed PDF shapes for mixture fraction, normalized enthalpy, and normalized progress variable with subgrid scalar PDF in an example DNS filter cell at t = 0.5 ms (top row) and t = 0.65 ms (bottom row).

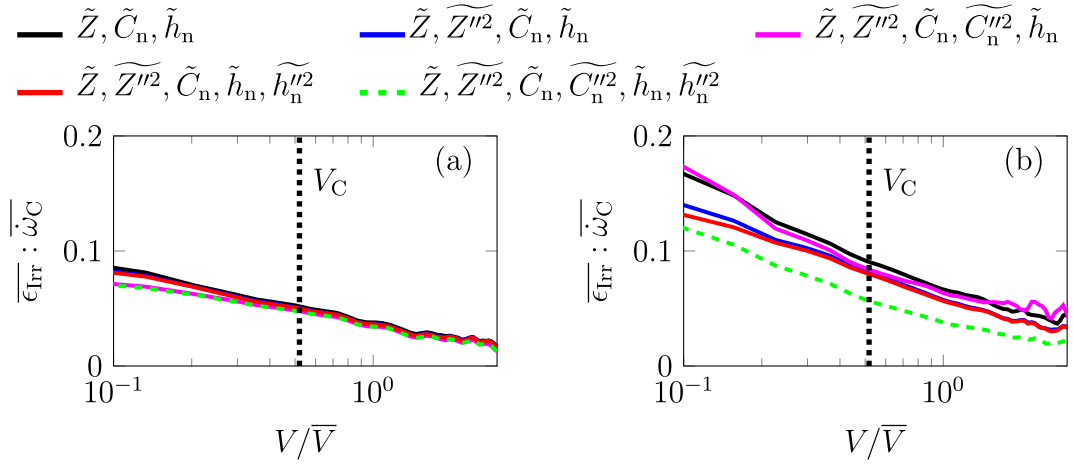

Fig. 12. Effect of adding the variance of different input parameters in the irreducible error of filtered progress variable source term at (a) t = 0.5 ms and (b) t = 0.65 ms. Volumes larger than V_C represent regions outside a cluster.

of using β-PDF in comparison with a δ function and the filtered model results. The δ function corresponds to not considering the sub-filter distributions in the model, and the filtered model inherently considers the correct sub-filter joint distributions of the DNS data without the assumption of presumed PDF shapes.

To this end, four different combinations of PDF shapes, as shown in Fig. 13, are applied. First, a δ function for all input scalars (3δ) is assumed. Then the typical assumption of a β distribution for mixture fraction while maintaining a δ function for progress variable and enthalpy (1β) serves as the reference model. In addition, the performance of the model is evaluated by employing β distribution for mixture fraction and progress variable (2β). Finally, a β distribution for all input parameters (3β) is investigated.

Fig. 13 shows the normalized functional errors for $\overline{\dot{\omega}_C}$. These errors are calculated based on Eqs. (4), (5), (6), and (11). The functional error for each PDF combination is compared with the respective error for the filtered FPV model results, which inherently considers the correct sub-filter joint distributions of the DNS data.

Around the ignition phase (t = 0.5 ms), all of the investigated PDF shapes exhibit comparable performance to the filtered FPV model results in predicting $\overline{\dot{\omega}_C}$. This finding aligns with the results from Fig. 12, which indicate that including variances as additional input parameters does not improve the errors. Hence, using the δ function as PDF shape for all input parameters can capture the ignition process as well as other models. This indicates that the distribution of sub-filters does not significantly affect the prediction of the progress variable source term during ignition, and the main contribution to the total modeling error is due to the performance of the non-premixed flamelet table.

However, towards the end of the ignition phase (t = 0.65 ms), the mixture fraction in the subgrid has a larger variance compared to the time of ignition. Consequently, it has a more pronounced influence on the PDF shapes, particularly within the particle clusters, as shown in Fig. 11. In these regions, the reference model 1β shows a better overall performance in predicting $\overline{\dot{\omega}_C}$. However, 2β and 3β models show worse predictions, which shows that choosing the β distributions for progress variable and enthalpy is not a good choice for predicting the quantity of interest in clustering particle cloud combustion.

The performance of different presumed PDF assumptions in predicting the quantity of interest is further analyzed in Fig. 14. Here, the prediction of $\overline{\dot{\omega}_C}$ using three models 3δ, 1β, and 3β is compared with the filtered FPV predictions.

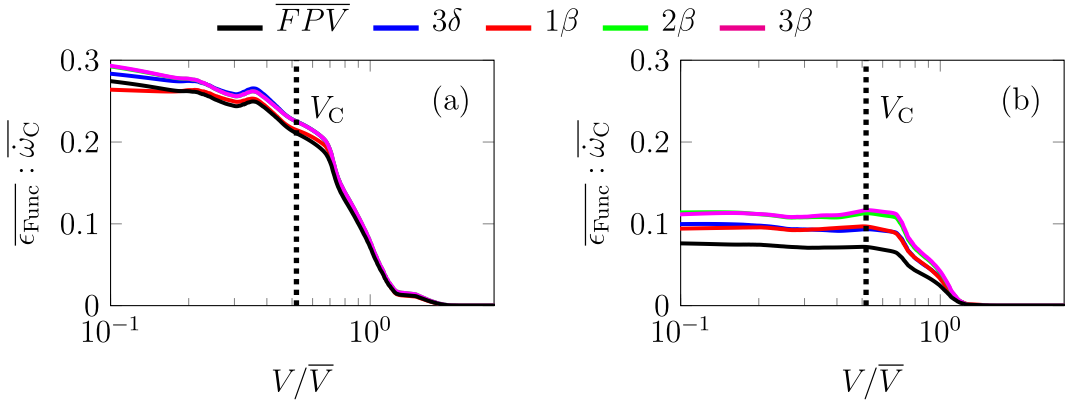

Fig. 13. Functional errors of filtered progress variable source term at (a) t = 0.5 ms and (b) t = 0.65 ms for different PDF assumptions in the FPV model. Volumes larger than V_C represent regions outside of clusters.

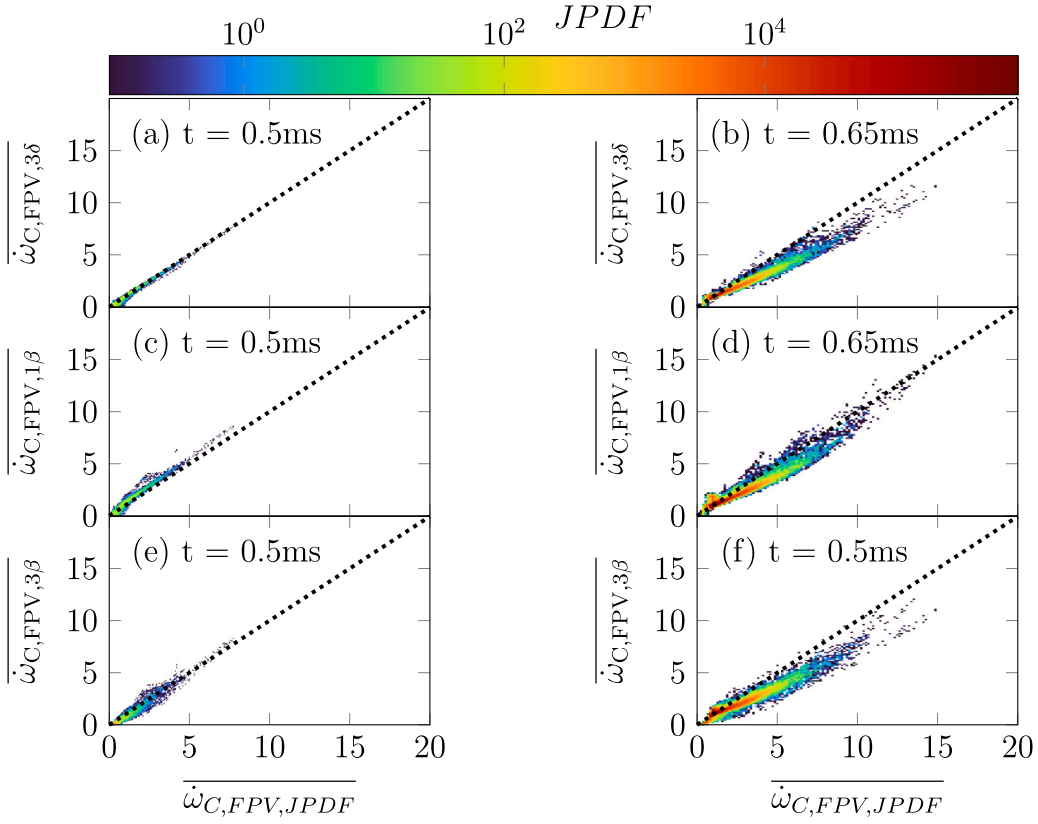

Fig. 14. Comparison between different PDF assumptions in the FPV model ($3\delta = \delta(\tilde{Z})\delta(\tilde{C})\delta(\tilde{h})$, $1\beta = \beta(\tilde{Z})$, and $3\beta = \beta(\tilde{Z})\beta(\tilde{C})\beta(\tilde{h})$) and the filtered-FPV prediction for progress variable source term ($\overline{\dot{\omega}_{C,FPV,JPDF}}$) at t = 0.5 ms and t = 0.65 ms.

This comparison is chosen to provide further insight into the effect of including input parameter distributions in the final prediction of the quantity of interest. Similar to the results from Fig. 13, Fig. 14 show that around ignition, all presumed PDF shapes show the same performance. However, at the end of the ignition process (t = 0.65 ms), using the 3δ and 3β model can lead to worse predictions compared to 1β model for higher progress variable source terms. This is due to incorrectly assumed PDF shapes at these conditions.

5. Conclusions

This study presents a comprehensive investigation of modeling the homogeneous ignition in clustering particle clouds in isotropic turbulence. For this purpose, a DNS of pulverized coal particles using the point-particle model for the dispersed phase and detailed chemical kinetics for the gas phase was performed.

Initially, auto-ignition was found at positions with favorable thermo-chemical states, followed by growing and merging the individual ignition kernels. It was observed that particle clustering has a significant impact on the ignition process. Ignition predominantly occurs in regions outside of the clusters, where higher temperatures are present due to reduced energy sink associated with particle heating. These ignition locations exhibit a lean mixture of released volatiles and oxidizer, resulting in lower scalar dissipation compared to the cluster locations.

This study employed a systematic error decomposition approach, utilizing the optimal estimator concept, to assess tabulated flamelet models in particle clustering conditions. The assessment focused on

determining the errors associated with the reference flamelet/progress variable (FPV) model inputs and evaluating its functional model performance both inside and outside of particle clusters. The assessment of the FPV model revealed its good performance in predicting the progress variable source term. However, around the ignition phase, a higher deviation from the prediction by the DNS data was observed, particularly for the progress variable source term inside particle clusters. This study identified an efficient set of input parameters that yields the smallest irreducible errors, consisting of mixture fraction Z, normalized progress variable C_n, and enthalpy hn. Not including the enthalpy resulted in higher errors, especially during the ignition phase, highlighting the increased sensitivity of quantity of interest to enthalpy in the ignition phase. Regarding the progress variable definition, it was found that including CO_2, CO, and O_2 as the set of parameters showed good performance in predicting the quantity of interest. Omitting either CO or O_2 led to a significant increase in functional modeling errors when predicting the progress variable source term. Also, replacing CO with H_2O improved the prediction of the progress variable source term during the ignition phase, especially inside the clusters.

The findings reveal that incorporating the variances of the input parameters improves the irreducible errors, especially inside particle clusters, primarily at the end of the ignition process, where the sub-filter distribution of the DNS data exhibits larger variances. In contrast, during the ignition onset, when individual kernels with small variances dominate due to particle clustering effects on ignition location, a δ function shows a good performance. However, in the case of functional errors, the presumed marginal PDF shape assumption is prone to errors originating from the shape function. Choosing the correct presumed PDF shape that matches the DNS sub-filter distribution is challenging and has an important impact on the model's performance.

CRediT authorship contribution statement

Pooria Farmand: Writing – review & editing, Writing – original draft, Visualization, Validation, Software, Resources, Methodology, Investigation, Formal analysis, Data curation, Conceptualization. **Hendrik Nicolai:** Writing – review & editing, Visualization, Resources, Methodology, Investigation, Formal analysis, Data curation, Conceptualization. **Muhammad Usman:** Visualization, Methodology, Investigation, Formal analysis. **Lukas Berger:** Writing – review & editing, Supervision, Resources, Methodology, Conceptualization. **Antonio Attili:** Writing – review & editing, Supervision, Methodology, Investigation, Conceptualization. **Michael Gauding:** Formal analysis, Investigation, Supervision, Writing – review & editing. **Christian Hasse:** Investigation, Project administration, Supervision, Writing – review & editing. **Heinz Pitsch:** Conceptualization, Funding acquisition, Methodology, Project administration, Supervision, Writing – review & editing.

Declaration of competing interest

The authors declare that they have no known competing financial interests or personal relationships that could have appeared to influence the work reported in this paper.

Data availability

The data that support the findings of this study are openly available and can be found at doi: http://dx.doi.org/10.5281/zenodo.11471198.

Acknowledgments

The authors kindly acknowledge financial support through Deutsche Forschungsgemeinschaft (DFG) Projektnummer 215035359 - through SFB/TRR 129. The authors also gratefully acknowledge the computing time provided to them at the NHR Center NHR4CES at RWTH Aachen University (project number p0020514 and p0021020), which is funded by the Federal Ministry of Education and Research, and the state governments participating on the basis of the resolutions of the GWK for national high performance computing at universities.

Appendix

The turbulence statistics for the studied isotropic turbulence configuration during different time instances are briefly summarized in Table 2. η and t_η are the respective Kolmogorov length and time scales,

Table 2
Turbulence statistics at different time instances.

Time [ms]	Re_λ	Re_{Turb}	η [m]	l_t [m]	t_η [ms]	t_l [ms]	St
0	30.7	141.8	1.04E−04	4.27E−03	4.47E−02	5.33E−01	6.199
0.46	30.9	143.9	9.94E−05	4.13E−03	4.16E−02	4.99E−01	6.207
0.5	30.5	140.1	9.96E−05	4.06E−03	4.27E−02	5.05E−01	6.333
0.55	29.4	129.8	1.01E−04	3.88E−03	4.34E−02	4.94E−01	6.032
0.6	28.5	122.1	1.02E−04	3.76E−03	4.46E−02	4.92E−01	5.775
0.65	27.7	115.2	1.04E−04	3.66E−03	4.48E−02	4.81E−01	5.365

and l_t and t_l correspond to integral length and time scales.

References

[1] Hasse C, Debiagi P, Wen X, Hildebrandt K, Vascellari M, Faravelli T. Advanced modeling approaches for CFD simulations of coal combustion and gasification. Prog Energy Combust Sci 2021;86:100938.
[2] Fletcher TH, Kerstein AR, Pugmire RJ, Grant DM. Chemical percolation model for devolatilization. 2. Temperature and heating rate effects on product yields. Energy Fuels 1990;4(1):54–60.
[3] Maffei T, Khatami R, Pierucci S, Faravelli T, Ranzi E, Levendis YA. Experimental and modeling study of single coal particle combustion in O_2/N_2 and Oxy-fuel (O_2/CO_2) atmospheres. Combust Flame 2013;160(11):2559–72.
[4] Nicolai H, Debiagi P, Wen X, Dressler L, Massmeyer A, Janicka J, et al. Flamelet LES of swirl-stabilized oxy-fuel flames using directly coupled multi-step solid fuel kinetics. Combust Flame 2022;241:112062.
[5] Farmand P, Nicolai H, Schumann C, Attili A, Berger L, Li T, et al. Numerical investigation and assessment of flamelet-based models for the prediction of pulverized solid fuel homogeneous ignition and combustion. Combust Flame 2022;235:111693.
[6] Rieth M, Clements A, Rabaçal M, Proch F, Stein O, Kempf A. Flamelet LES modeling of coal combustion with detailed devolatilization by directly coupled CPD. Proc Combust Inst 2017;36(2):2181–9.
[7] Nicolai H, Debiagi P, Janicka J, Hasse C. Flamelet LES of oxy-fuel swirling flames with different O_2/CO_2 ratios using directly coupled seamless multi-step solid fuel kinetics. Fuel 2023;344:128089.
[8] Fletcher TH. Review of 30 years of research using the chemical percolation devolatilization model. Energy Fuels 2019;33(12):12123–53.
[9] Yin C, Yan J. Oxy-fuel combustion of pulverized fuels: Combustion fundamentals and modeling. Appl Energy 2016;162:742–62.
[10] Stein O, Olenik G, Kronenburg A, Cavallo Marincola F, Franchetti B, Kempf A, et al. Towards comprehensive coal combustion modelling for LES. Flow Turbul Combust 2013;90:859–84.
[11] Nicolai H, Wen X, Miranda F, Zabrodiec D, Massmeyer A, Di Mare F, et al. Numerical investigation of swirl-stabilized pulverized coal flames in air and oxy-fuel atmospheres by means of large eddy simulation coupled with tabulated chemistry. Fuel 2021;287:119429.
[12] Nicolai H, Kuenne G, Knappstein R, Schneider H, Becker L, Hasse C, et al. Large Eddy Simulation of a laboratory-scale gas-assisted pulverized coal combustion chamber under oxy-fuel atmospheres using tabulated chemistry. Fuel 2020;272:117683.
[13] Wen X, Nicolai H, Schneider H, Cai L, Janicka J, Pitsch H, et al. Flamelet LES of a swirl-stabilized multi-stream pulverized coal burner in air and oxy-fuel atmospheres with pollutant formation. Proc Combust Inst 2021;38(3):4141–9.
[14] Rieth M, Proch F, Rabaçal M, Franchetti B, Marincola FC, Kempf A. Flamelet LES of a semi-industrial pulverized coal furnace. Combust Flame 2016;173:39–56.
[15] Watanabe J, Yamamoto K. Flamelet model for pulverized coal combustion. Proc Combust Inst 2015;35(2):2315–22.
[16] Nicolai H, Li T, Geschwindner C, di Mare F, Hasse C, Böhm B, et al. Numerical investigation of pulverized coal particle group combustion using tabulated chemistry. Proc Combust Inst 2021;38(3):4033–41.
[17] Knappstein R, Kuenne G, Ketelheun A, Köser J, Becker L, Heuer S, et al. Devolatilization and volatiles reaction of individual coal particles in the context of FGM tabulated chemistry. Combust Flame 2016;169:72–84.
[18] Dressler L, Sacomano Filho FL, Ries F, Nicolai H, Janicka J, Sadiki A. Numerical prediction of turbulent spray flame characteristics using the filtered Eulerian stochastic field approach coupled to tabulated chemistry. Fluids 2021;6(2):50.

[19] Tufano G, Stein O, Wang B, Kronenburg A, Rieth M, Kempf A. Coal particle volatile combustion and flame interaction. Part I: Characterization of transient and group effects. Fuel 2018;229:262–9.
[20] Tufano G, Stein O, Wang B, Kronenburg A, Rieth M, Kempf A. Coal particle volatile combustion and flame interaction. Part II: Effects of particle Reynolds number and turbulence. Fuel 2018;234:723–31.
[21] Messig D, Vascellari M, Hasse C. Flame structure analysis and flamelet progress variable modelling of strained coal flames. Combust Theory Model 2017;21(4):700–21.
[22] Wen X, Luo K, Jin H, Fan J. Numerical investigation of coal flamelet characteristics in a laminar counterflow with detailed chemistry. Fuel 2017;195:232–42.
[23] Luo K, Wang H, Fan J, Yi F. Direct numerical simulation of pulverized coal combustion in a hot vitiated co-flow. Energy Fuels 2012;26(10):6128–36.
[24] Bai Y, Luo K, Qiu K, Fan J. Numerical investigation of two-phase flame structures in a simplified coal jet flame. Fuel 2016;182:944–57.
[25] Hara T, Muto M, Kitano T, Kurose R, Komori S. Direct numerical simulation of a pulverized coal jet flame employing a global volatile matter reaction scheme based on detailed reaction mechanism. Combust Flame 2015;162(12):4391–407.
[26] Rieth M, Kempf A, Kronenburg A, Stein O. Carrier-phase DNS of pulverized coal particle ignition and volatile burning in a turbulent mixing layer. Fuel 2018;212:364–74.
[27] Wen X, Rieth M, Scholtissek A, Stein OT, Wang H, Luo K, et al. A comprehensive study of flamelet tabulation methods for pulverized coal combustion in a turbulent mixing layer—part I: A priori and budget analyses. Combust Flame 2020;216:439–52.
[28] Wen X, Rieth M, Scholtissek A, Stein OT, Wang H, Luo K, et al. A comprehensive study of flamelet tabulation methods for pulverized coal combustion in a turbulent mixing layer—Part II: Strong heat losses and multi-mode combustion. Combust Flame 2020;216:453–67.
[29] Rieth M, Kempf AM, Stein OT, Kronenburg A, Hasse C, Vascellari M. Evaluation of a flamelet/progress variable approach for pulverized coal combustion in a turbulent mixing layer. Proc Combust Inst 2019;37(3):2927–34.
[30] Brosh T, Patel D, Wacks D, Chakraborty N. Numerical investigation of localised forced ignition of pulverised coal particle-laden mixtures: a direct numerical simulation (DNS) analysis. Fuel 2015;145:50–62.
[31] Krüger J, Haugen NE, Mitra D, Løvås T. The effect of turbulent clustering on particle reactivity. Proc Combust Inst 2017;36(2):2333–40.
[32] Farazi S, Hinrichs J, Davidovic M, Falkenstein T, Bode M, Kang S, et al. Numerical investigation of coal particle stream ignition in oxy-atmosphere. Fuel 2019;241:477–87.
[33] Attili A, Farmand P, Schumann C, Farazi S, Böhm B, Li T, et al. Numerical simulations and experiments of ignition of solid particles in a laminar burner: Effects of slip velocity and particle swelling. Flow Turbul Combust 2020;1–17.
[34] Li T, Farmand P, Geschwindner C, Greifenstein M, Köser J, Schumann C, et al. Homogeneous ignition and volatile combustion of single solid fuel particles in air and oxy-fuel conditions. Fuel 2021;291:120101.
[35] Cai L, Kruse S, Felsmann D, Pitsch H. A methane mechanism for oxy-fuel combustion: Extinction experiments, model validation, and kinetic analysis. In: Flow turbulence and combustion. Springer; 2020.
[36] Wen X, Shamooni A, Stein OT, Cai L, Kronenburg A, Pitsch H, et al. Detailed analysis of early-stage NOx formation in turbulent pulverized coal combustion with fuel-bound nitrogen. Proc Combust Inst 2021;38(3):4111–9.
[37] Wen X, Nicolai H, Stein OT, Janicka J, Kronenburg A, Hasse C. Effects of air and oxy-fuel atmospheres on flamelet modeling of pollutant formation in laminar counterflow solid fuel flames. Fuel 2021;285:119079.
[38] Farazi S, Attili A, Kang S, Pitsch H. Numerical study of coal particle ignition in air and oxy-atmosphere. Proc Combust Inst 2019;37(3):2867–74.
[39] Grant DM, Pugmire RJ, Fletcher TH, Kerstein AR. Chemical model of coal devolatilization using percolation lattice statistics. Energy Fuels 1989;3(2):175–86.
[40] Jimenez S, Gonzalo-Tirado C. Properties and relevance of the volatile flame of an isolated coal particle in conventional and oxy-fuel combustion conditions. Combust Flame 2017;176:94–103.
[41] Goodwin DG, Speth RL, Moffat HK, Weber BW. Cantera: An object-oriented software toolkit for chemical kinetics, thermodynamics, and transport processes. 2021, http://dx.doi.org/10.5281/zenodo.4527812, Version 2.5.1, https://www.cantera.org.
[42] Pierce CD, Moin P. Progress-variable approach for large-eddy simulation of non-premixed turbulent combustion. J Fluid Mech 2004;504:73–97.
[43] Wollny P, Rogg B, Kempf A. Modelling heat loss effects in high temperature oxy-fuel flames with an efficient and robust non-premixed flamelet approach. Fuel 2018;216:44–52.
[44] Ketelheun A, Kuenne G, Janicka J. Heat transfer modeling in the context of large eddy simulation of premixed combustion with tabulated chemistry. Flow Turbul Combust 2013;91:867–93.
[45] Fiorina B, Gicquel O, Vervisch L, Carpentier S, Darabiha N. Premixed turbulent combustion modeling using tabulated detailed chemistry and PDF. Proc Combust Inst 2005;30(1):867–74.
[46] Landenfeld T, Sadiki A, Janicka J. A turbulence-chemistry interaction model based on a multivariate presumed beta-pdf method for turbulent flames. Flow Turbul Combust 2002;68(2):111–35.
[47] Olbricht C, Stein O, Janicka J, Van Oijen J, Wysocki S, Kempf A. LES of lifted flames in a gas turbine model combustor using top-hat filtered PFGM chemistry. Fuel 2012;96:100–7.
[48] Berger L, Kleinheinz K, Attili A, Bisetti F, Pitsch H, Mueller ME. Numerically accurate computational techniques for optimal estimator analyses of multi-parameter models. Combust Theory Model 2018;22(3):480–504.
[49] Trisjono P, Pitsch H. Systematic analysis strategies for the development of combustion models from DNS: A review. Flow Turbul Combust 2015;95:231–59.
[50] Moreau A, Teytaud O, Bertoglio J-P. Optimal estimation for large-eddy simulation of turbulence and application to the analysis of subgrid models. Phys Fluids 2006;18(10):105101.
[51] Fessler JR, Kulick JD, Eaton JK. Preferential concentration of heavy particles in a turbulent channel flow. Phys Fluids 1994;6(11):3742–9.
[52] Obligado M, Teitelbaum T, Cartellier A, Mininni P, Bourgoin M. Preferential concentration of heavy particles in turbulence. J Turbul 2014;15(5):293–310.
[53] Monchaux R, Bourgoin M, Cartellier A. Analyzing preferential concentration and clustering of inertial particles in turbulence. Int J Multiph Flow 2012;40:1–18.
[54] Ying S, Xu G, Li C, Mao Z. Point cluster analysis using a 3D Voronoi diagram with applications in point cloud segmentation. ISPRS Int J Geo-Inf 2015;4(3):1480–99.
[55] Palmore Jr JA, Desjardins O. Technique for forcing high Reynolds number isotropic turbulence in physical space. Phys Rev Fluids 2018;3(3):034605.
[56] Lau T, Nathan GJ. The influence of Stokes number on particle clustering within a two-phase turbulent jet. In: 7th Australian conference on laser diagnostics in fluid mechanics and combustion. 2015.
[57] Gualtieri P, Picano F, Casciola C. Anisotropic clustering of inertial particles in homogeneous shear flow. J Fluid Mech 2009;629:25–39.
[58] Wen X, Rieth M, Han W, Chen JH, Hasse C. Investigation of the ignition processes of a multi-injection flame in a diesel engine environment using the flamelet model. Proc Combust Inst 2021;38(4):5605–13.
[59] Cant S. SB pope, turbulent flows, cambridge university press, cambridge, UK, 2000, 771 pp. Combust Flame 2001;4(125):1361–2.
[60] Apte S, Mahesh K, Lundgren T. Accounting for finite-size effects in simulations of disperse particle-laden flows. Int J Multiph Flow 2008;34(3):260–71.
[61] Wang B, Kronenburg A, Tufano GL, Stein OT. Fully resolved DNS of droplet array combustion in turbulent convective flows and modelling for mixing fields in inter-droplet space. Combust Flame 2018;189:347–66.